FPRINT-94-20

FPRINT-94-20

Fermilab Library
0 1160 0033144 1

Status Report

ν^s

CP–Violation in $K^{\pm} \to \pi^{\pm}\pi^{0}\pi^{0}$ Decays

FERMILAB
MAR 24 1994
LIBRARY

TNF–Collaboration

DESY–Group

16.3.93

NAME	ID No.	M.S.

RETURN TO FERMILAB LIBRARY

Introduction

The aim of the following pages is to give an account of the ongoing work in the Serpukhov $K^{\pm}$–decay experiment, which was concipated two years ago [1] as a straight and promising means to find a CP-violating charge asymmetry in the Dalitz-plot slope factors for $K^{\pm} \to \pi^{\pm}\pi^{0}\pi^{0}$ decays.

The theoretical estimates of the effect [3] have been subject to some criticisms [4]. New and more refined calculations [5] have lead to predictions similar to the first mentioned ones. At the same time it was possible to trace more clearly the origin for this enhancement.

Usually there are given quantitative results only in the soft pion limit, where the effect of CP-violation is determined by the weak phase difference between $\Delta I = \frac{1}{2}$ and $\Delta I = \frac{3}{2}$ transition amplitudes and therefore – as in the case of $K^0 \to 2\pi$ decays–suppressed by the $\Delta I = \frac{1}{2}$ rule. In our case there appears a weak phase difference also between the two $\Delta I = \frac{1}{2}$ transition amplitudes to both the 3π – final states with $I = 1$ at tree level (in p^4 – order of the chiral expansion), which is connected to a piece $\sim$ tr $(\lambda_a \partial^2 U^{(+)})$ (see [5] and the definitions given there) in the scalar mesonic current. This term was introduced by [6] to describe the splitting of the decay constants $F_{K,\pi}$ and it appears naturally in the bosonization approach given in [7]. It enters the effective weak interaction lagrangian via the hadronized form of the penguin diagram, which is responsible for direct CP–violation, according to the Standard model.

In quantitative respect, a further important ingredient is the strong phase difference between the above mentioned final states, which appears sizeable (of order 1) from explicit loop calculations (compare also [9]), while alternative approaches [8] based on unitary cutting rules, with some approximations, lead to values lower by an order of magnitude. While this point deserves further investigation, one should consider as well the possibility of experimental determination by fitting all known $K \to 3\pi$ channels with complex isotopic amplitudes in the manner of [10] relying on more precise experimental data for linear and quadratic Dalitz–plot slopes. Until now, such fits are not sufficiently sensitive to these phases. But since the K^0–data are improving considerably and the channel $K^{\pm} \to \pi^{\pm}\pi^{+}\pi^{-}$ is quite well measured, it is just the channel $K^{\pm} \to \pi^{\pm}\pi^{0}\pi^{0}$, which is least well measured. A sample of $\sim 10^5$ reconstructed events would already mean a significant improvement. This should be the first goal of this experiment.

For the channel in question here, the asymmetry

$$\Delta g = \frac{g(K^+) - g(K^-)}{g(K^+) + g(K^-)}$$

is expected to be found in the region $0.2|\varepsilon'/\varepsilon| < \Delta g < 0.7|\varepsilon'/\varepsilon|$ (see fig.1) depending on the value of the top-mass. If we assume for $|\varepsilon'/\varepsilon|$ a value consistent with latest measurements, $(2.2 \pm 1.1) \times 10^{-3}$ [11] we may hope to get here for the first time an effect of CP–violation outside the K^0–system, being at the same time an unambiguous evidence against the Superweak model [12] and in favour of direct CP–violation in the framework of the Standard model. While it is clear, that this very ambitious goal justifies a significant effort for its accomplishment, it was not clear at the beginning–and is not clear now–if it will be possible to reach the interesting level of $10^{-3} \div 10^{-4}$ in systematical and statistical accuracy for g with the actual equipment. Any reliable conclusion can be drawn only after the evaluation of a substantial part of the statistics and a complete exploration of the apparatus.

A specific feature of this experiment is the fact, that it uses part of detectors of the Neutrino–tagging–experiment, namely the beam part and the tagging station. A description of this equipment has been given in the first proposal and–in a more actual version–in the proposal for this experiment [2]. Although, at the time of that publication, the main parts have just been starting

to work, there is not included information on the actual performance of our detectors, because it was rapidly changing in the process of adjustment and calibration.

In the last running periods (December 91–April 92) we received further test data. Especially in the April run it was possible, after a new adjustment of the beam and recalibration of the electromagnetic calorimeter, for the first time to record some significant statistics with and without trigger and for both beam polarities.

Our strategy was, to go as far as possible in evaluating these data, without too much emphasis on complete statistics and corrections for special cases, in order to find out any difficulties as early as possible.

In the following we give a short and incomplete account of these preliminary results.

Status of hodoscopes

The 3 x–y–hodoscopes (of element width 14 mm) have been fully operational during the last runs. In addition, a fourth hodoscope with the same structure of x–y–planes, placed behind the e. m. calorimeter, has taken data for the first time in the April 92 run. A technical description of these devices can be found in [2].

The trajectory of the beam particle was measured by two x, y–hodoscopes upstream of the decaytube with effective element width 5 mm.

Alignment procedure

The longitudinal (z)–positions of all detectors (including the e. m. calorimeter) are fixed by geodetic measurements. These were not sufficient for a precise determination of the relative transverse (x, y) positions, which had to be found by comparing the hit-positions for single tracks crossing all the detectors.

A special procedure was used to check the relative positions of the z–axis for up–stream (beam-) and down–stream (secondary) hodoscopes. For a sample of well reconstructed $K^+ \rightarrow \pi^+\pi^0$ decays, we compared event by event the direction of the total momentum of the decay particles with the K^+ direction from the beam hodoscopes. After the necessary correction of the relative direction of both z–axis in the next step we compared the vertex z–distributions of $K^+ \rightarrow \mu^+\nu$ decays for positive and negative projected decay angles (in both the x–z and the y–z planes). They appear to be shifted with respect to each other, if the z–axis up–stream and down–stream are displaced by a parallel shift.

Because all checks can be done with virtually unlimited statistical accuracy, we consider these alignment problems as practically solved. The residual errors are probably given by time dependent instabilities and will be studied by comparisons between different running periods. An additional geodetic control measurement of the z–positions is foreseen.

Efficiency

After a software track finding procedure was realized, which finds and matches secondary track projections in both x– and y–planes, using additional information like angular cuts from kinematics, finding tracks with all 6 hits seen, and also tracks with one hit missing (under conditions, which avoid ambiguities), it has been possible, by comparing both samples of tracks, to estimate the efficiency in a localized way. That means, we plotted for each plane the positions of track crossings, where the corresponding hit was missing.

For the last (April 92) run, we found a mean efficiency for the secondary hodoscopes of $\bar{\varepsilon} = 83\%$ (for 17% of tracks one hit was missing). Because this efficiency is weighted with the actual distribution of hits in each plane, it is not the same as the overall efficiency of the detector elements, because the inner, less efficient, parts of the hodoscopes are decisive. Nevertheless it is just this figure which is needed for correction of experimental results.

The overall efficiency ε_t of track reconstruction would then be

$$\varepsilon_t = \bar{\varepsilon}^6 + 6\bar{\varepsilon}^5(1 - \bar{\varepsilon}) = 0.73.$$

In the next reconstruction step, for events, where at least one secondary track has been found, we fixed the vertex by calculating the point of closest approach either to the primary track or to the beam–axis (a geometrical vertex fit procedure is also available, but for reasons of simplicity has not been used at this stage).

In fig.2 a,b we show the vertex – z distributions for minimum bias events, together with the corresponding M.C. distribution for $K^{\pm} \rightarrow \pi^{\pm}\pi^0\pi^0$ decays. The downstream end of the decay tube is at $z = 0$, it starts at $z = -5850$ cm.

We don't see a significant background from upstream events or beam halo. The drop for $z \rightarrow 0$ is more pronounced for the signal channel, because it has smaller angles of the charged track, than, f.i., the prominent $K \rightarrow \mu\nu$ decay.

The efficiency of the vertex reconstruction is found to be

$$\varepsilon_V = 0.37$$

For our track– and vertex finding procedures, we would expect

$$\varepsilon_V^{M.C.} = 0.82$$

for $\varepsilon_t = 1$, that means $\varepsilon_V = 0.82\ \varepsilon_t = 0.6$. The additional reduction has to be ascribed to triggers from other sources (combinatorial background associated with beam spikes, wrong triggers etc.). This point will be further investigated.

Calibration of the electromagnetic calorimeter

In our experiment, all dynamical information about the final state is based solely on the calorimetric energy measurements for the γ_s from π^0 decays. Therefore the calibration of the calorimeter requires careful and continuous study. Especially after the adjustment of the analog signals from the calorimeter blocks (to be used in the trigger, see below), which was done by changing the HV by means of servomotors, a complete recalibration has been done before and some additional checks after the last running period.

The calibration procedure is described in [2]. Each channel is characterized by one calibration coefficient. A further characteristic is its threshold value, which is adjusted in relation to the pedestal width. Until now, the leakage problem due to this energy cuts has not been studied in detail. The following results on π^0-masses are uncorrected.

For the further treatment of the data we used a simple peak finding algorithm. It starts with the block of highest energy, attaches to it any energy found in its 8 neighboring blocks, and finds the peak coordinates as the energy weighted mean value (center of gravity), then continues with the next energetic block left and so on. This procedure is adequate for γ(or e)-hits, but sometimes fails for wide clusters due to interacting hadrons. Therefore, for any cluster, also the dispersion of the energy distribution is calculated. This may by used in a later stage to improve the $\pi - e$–separation.

In order to test the calibration and the energy resolution, we selected a sample of $K^- \to \pi^-\pi^0$ decays, requiring a reconstructed hadron track resp. vertex and two γ-clusters in the e. m. calorimeter. Furthermore, from the energy-momentum balance we could include an additional cut on the residual transverse momentum ($p_t < 0.05$ GeV).

In fig.3 a,b,c we show the π^0–mass distribution without p_t–cut, with $p_t < 0.05 GeV$ and with background subtraction (about 20 events/channel) respectively.

From the last distribution, the mean value of 130.3 MeV is slightly but significantly too small. The fit to a gaussian gives a standard deviation of 16.3 MeV corresponding to an error of the mean value of 0.5 MeV. We suppose, that this shift is caused by energy leakage due to a cut of 1 GeV used for defining hits in the e.m. calorimeter. This question will be studied later.

The relative mass resolution is found as

$$\frac{\Delta m_\pi}{m_\pi} = 0.125$$

In order to study the influence of energy– and angular resolution resp. on the π^0–mass resolution of our calorimeter, we took from M.C. simulation (see fig.4 a,b) the errors for the projected angles of γs

$$\Delta\delta_{x,y} = 1.6\,\mathrm{mrad}$$

(neglecting here the dependence on γ–energies), resulting in the error

$$\Delta\Theta = 2\Delta\delta_{x,y} = 3.2\,\mathrm{mrad}$$

for the spatial angle between two γs. From the relation :

$$m_\pi^2 \approx E_1 E_2 \Theta^2, \quad E_{1,2} : \gamma - \text{energies}$$

we find for a given π^0–energy $E = E_1 + E_2$ the mean value of Θ (taking into account, that the spectra of $E_{1,2}$ are constant: $E_1 = \xi E$, $E_2 = (1-\xi)E$, with ξ equally distributed between 0 and 1)

$$\bar{\Theta} = \int_0^1 d\xi \frac{m_\pi}{\sqrt{\xi(1-\xi)}} \frac{1}{E} = \pi \frac{m_\pi}{E}$$

From error propagation we have

$$\frac{\Delta m_\pi}{m_\pi} = \frac{1}{2}\frac{\Delta(E_1E_2)}{E_1E_2} \oplus \frac{\Delta\Theta}{\Theta} = 0.125$$

and, for $\Theta = \bar{\Theta}$, and E measured in GeV,

$$\frac{\Delta\Theta}{\Theta} \sim 7.55 \cdot 10^{-3} E$$

On the other hand, the contribution of the energy resolution may be estimated, supposing $\frac{\Delta E_i}{E_i} = \frac{C}{\sqrt{E_i}}$, as

$$\frac{1}{2}\frac{\Delta(E_1E_2)}{E_1E_2} = \frac{1}{2}\left(\frac{\Delta(E_1)}{E_1} \oplus \frac{\Delta(E_2)}{E_2}\right) = \frac{C}{2}\left(\frac{1}{\sqrt{E_1}} \oplus \frac{1}{\sqrt{E_2}}\right)$$

$$= \frac{C}{2}\sqrt{\frac{E_1+E_2}{E_1E_2}} = \frac{C}{2}\frac{\sqrt{E}}{m_\pi/\Theta} = \frac{C}{2}\frac{\pi}{\sqrt{E}}$$

The combined relative error of the π^0–mass is given in fig.5 as a function of E, in the kinematic domain for 2π–decays, for C=0.2 and C=0.1 $\sqrt{GeV}$, respectively. The measured value $\frac{\Delta m_\pi}{m_\pi} =$

0.125, also shown in this fig. , excludes coefficients $C > 0.2\sqrt{GeV}$, and may be consistent with $C \sim 0.1\sqrt{GeV}$, where the resolution becomes equal to the measured one just at the mean π^0–energy of 16 GeV. In any case the optimal resolution is found near to the mean π^0–energy in $K \rightarrow 3\pi$ decays, being of the order 10 GeV, and should be even better than that observed for $K \rightarrow 2\pi$ decays.

Performance of Total–Sum Trigger

As described in [2], the event selection is being performed by two trigger levels: The first ("minimum bias") includes beam–scintillation, –Cerenkov and anticounter, selecting decaying $K^{\pm}$–mesons, and the second being derived from total analog sums of signals taken over "hexants" (quarters of quadrants) of the e.m. calorimeter. The latter has been used in the april 92 run for the first time. This required a readjustment of the HV of all channels with the help of the 10 GeV e^-–beam also used for calibration. For this purpose, the analog signals have been digitized and analyzed by the host computer, which resulted in appropriate steering signals for the servomotors changing the HV.

Of course, the calibration coefficients for the digital channels had to be redetermined afterwards by the standard procedure described in [2]. In order to fix the trigger–threshold for each hexant, the 10 GeV e^-–beam was used once more to measure the trigger rate as a function of the threshold. The drop of this threshold curve (the 50 % value) served then as the calibration point to fix the threshold scale.

For the control of the trigger performance, the analog sums for all hexants are also included in the data record for each triggered event. In fig.6 their recorded and digitized values, in arbitrary scale, are plotted against the measured energy per hexant (given on the vertical axis). One finds an overall linear correlation despite some deficits: a band near the vertical axis, caused by ineffective analog channels, and some horizontal bands, at 7.0 and 12.5 GeV, probably due to noisy signal channels.

In general, the threshold for each hexant was fixed at the value corresponding to 1 GeV. The trigger requirement was than generally to have at least two hexants above threshold. This is a more inclusive requirement than foreseen in the proposal [2], but it just saturated the actual data taking capability (about 200 events/s) for the given beam intensity (10^6 /s).

Results of the april 92 – run

During this running period, about 3 days of the beam time have been spent for K–decays, mostly for various adjustments and calibrations of the detectors. The time used for data taking was about 50 hours, with a data taking rate of 150 triggers per burst. The beam and trigger conditions for the various runs have been the following:
- run No. 33, mini–bias trigger, K^-
- run No. 34–41, 2 hexants > 1 GeV trigger, K^-
- run No. 42, mini–bias trigger, K^-
- run No. 43–45, 2 hexants > 1 GeV trigger, K^+

The raw data were recorded on magnetic tapes by the experiment computer and thereafter rewritten at the main computer into the agreed transportable data structure (Z–BOOK, EPIO) and, f.i., given to EXABYTE cassettes. The data processing chain consists of the following parts:
- evaluation of the track–information from the hodoscopes

Table 1: Event statistics

Run: $K^- \to \pi^-\pi^0\pi^0$	M. C. generated: 88300 Minibias: 56057			Minibias - 76488			2nd l. tr. (NHEX ≥ 2) (hardware) 99767		
2nd l. tr.: NHEX (software)	< 2	2	>2	<2	2	>2	<2	2	>2
	4968	17913	33194	60046	4561	6236	10911	50029	38827
Vertex found	3595	14336	27991	22446	3930	2320	3181	18808	14293
4/5 clusters	-	1005	15850	15	36	446	-	230	2916
selected for fit	-	263	7098	12	12	195	-	85	1288
"fitted"	-	240	6171	-	-	77	-	-	517
$\chi^2 < 80$	-	210	5238	-	1	33	-	9	193
	-	5446			34			202	

- evaluation of the hit–information from the e.m. calorimeter
- selection of candidates for $K^\pm \to \pi^\pm\pi^0\pi^0$ decays
- kinematical fit
- output of HBOOK–information, N–tuples etc., for analysis with PAW

The input can be switched to files produced by M.C.–simulation without any changes. Events from data files and M.C. files can also be looked at by a viewing program. A sample of typical 3π–events is given in the appendix. The selection steps were the following:

1. vertex found: at least 1 charged secondary track reconstructed, the vertex is taken as the point of closest approach to the primary from all secondaries, if the distance is less than 10 cm (if the primary track has not been uniquely reconstructed, the best fitting beam axis is taken instead). This procedure will be replaced later by a standard geometrical vertex fit.

2. 4 or 5 clusters: selection of events with 4 or 5 clusters found after the cluster algorithm in the e.m. calorimeter.

3. events fulfilling the following conditions are selected for the fit:
   $N_{track} = 1$, $N_{cluster} = 4$, track does not point to cluster
   $N_{track} = 1$, $N_{cluster} = 5$, track does point to cluster (interacting $\pi^\pm$ is assumed)
   $N_{track} > 1$, $N_{cluster} = 4$, at least 1 track does not point to cluster

4. "fitted": kinematical fit (5 constraints) does not fail for one of the following reasons: the missing energy in the lab. or CMS system is less than the $\pi^\pm$–mass or $\chi^2 > 10^4$

5. χ^2–criterion (not finally adjusted until now).

The following figures are based on a sample of about 20% of the statistics (1 minimum bias run, 1 trigger run and 1 M.C. run) In table 1 we give the nb of events after the various selection steps for each of the above samples:

If we compare the figures in the last line with the number of triggers taken, we find a netto efficiency of 202/99767 = 0.2% (reconstructed events/triggered events) for the run with 2nd–level trigger condition NHEX$\geq$ 2, compared to 34/76488 = 0.04% for the run with minimum bias trigger only. This enrichment by a factor 5 from the 2nd level trigger is not the finally expected one for a trigger condition NHEX> 2, as foreseen in the earlier M.C. studies. In the latter case we would have found 193/38827 = 0.5%, that means an enrichment factor of 12.5. Therefore, the trigger concept should be considered as successful.

In order to make contact to our M.C. results, we are forced to introduce two corrections:

1. the efficiency of the vertex reconstruction $\varepsilon_V^{MC} = 82\%$ has to be replaced by the real value $\varepsilon_V = 37\%$, as discussed in chapter 1.

2. to the background from kaon decays is to be added background from other sources, only partially known at present (f.i. from combined events, especially connected with beam spikes, where, with a rate of 7%, events with more than 5 hits in the first hodoscope plane are seen).

From our data, we will only derive the signal to background rate S/B rate after the minimum bias and the 2nd level trigger. From

$$n_{1,2} = \left(\frac{S}{B+S}\right)_{1,2} \cdot \frac{\varepsilon_V}{\varepsilon_V^{MC}} \cdot \varepsilon_{1,2}^{MC} \cdot N_{1,2}$$

where $N_{1,2}$ is the number of triggers, $\varepsilon_1^{MC} = 9.7\%$ and $\varepsilon_2^{MC} = 16\%$ the reconstruction efficiency from M.C. with the minimum bias and the 2nd level trigger (NHEX> 2) respectively, and $n_{1,2}$ is the number of actually reconstructed events we find

$$\left(\frac{S}{B}\right)_1 = 1.0\% \quad \left(\frac{S}{B}\right)_2 = 7.0\%$$

In case of pure K-decays we would expect

$$Br \cdot \varepsilon_{MB}^{MC} = 1.1\% < \left(\frac{S}{B}\right)_1 < Br = 1.73\%$$

where $\varepsilon_{MB}^{MC} = \frac{56057}{88300} = 0.635$ is the suppression factor of the $\pi^{\pm}\pi^0\pi^0$ decays by the anticounter (the lower limit corresponds to unsuppressed, the upper to equally suppressed background). Correspondingly, from the old M.C. calculations, without additional background besides K^- decays, and using $(S/B)_1 = 1.73\%$, we expect (see [2], fig 5)

$$\left(\frac{S}{B}\right)_2^{old\,MC} = 22\%$$

The final rate of reconstructed events was estimated there, using $\varepsilon_2^{oldMC} = 23\%$ as $(S/B)_2 \cdot \varepsilon_2 = 5\%$. It is now reduced by one order of magnitude due to the following factors:

1. efficiency of the vertex reconstruction $\varepsilon_V/\varepsilon_V^{MC} = 0.45$

2. change of S/B : 7%/22% = 0.30

3. change of ε_2^{MC} : 16%/23% = 0.70

There is certainly room for improvements concerning factor 3., because, as remarked in the introduction, selection procedures, geometrical reconstruction and fit–adjustments are very preliminary.

Factor 2. is determined by beam conditions. For the K^+ run 44, being not included in the above sample, we found $(S/B)_2 = 15\%$.

Concerning factor 1., the overall efficiency of 73% for a 5 or 6–fold coincidence in the secondary hodoscopes sets some limit. Improvements are possible especially for the beam hodoscopes; for the secondary hodoscopes one could try to use kinematical constraints using the signals from the e.m. calorimeter, f.i., finding the decay plane for the charged π from the K and π^0 data, and looking for hit information in the corresponding region, thus reducing the requirements for pattern recognition.

For the final measurement of the slope parameter g we need the actual efficiency distribution over the Dalitz–plot from M.C. This is shown for a sample of 88300 generated $K^- \rightarrow \pi^-\pi^0\pi^0$ decays in fig.7a .

The projection on the Y-axis is given for the distribution of finally selected and reconstructed values . Whereas the drop for large Y after minimum bias selection is to be expected (due to cutting of small $\pi^{\pm}$–angles) there seems to be a further rise for small Y (with respect to a constant distribution to be compared with), which remains to be studied in detail. For real events, the Dalitz–plot Y distribution is shown in fig.7b, also with Dalitz plot contour correction, in the same form as fig. 7a. A straightforward Maximum Likelihood estimate of g is found from the equation (compare [2])

$$S(g) = \frac{1}{n}\frac{\partial ln\mathcal{L}}{\partial g} = \frac{1}{n}\sum \frac{n_i Y_i}{1+gY_i} - \frac{< Y >}{1+g < Y >} = 0 \ , n = \sum n_i$$

where n_i, Y_i are taken from hist. 7b, and $< Y >= -0.3215$ is the first moment from hist.7a (The error σ_g is related to the slope of the function given above as $\sigma_g^{-2} = -n\frac{dS}{dg}$. In fig.8 $S(g)$ is plotted as a function of g, and from the crossing point we derive

$$g = 0.66 \pm 0.06$$

not in disagreement with the current value $g = 0.594 \pm 0.019$. Alternatively, we can weight the Dalitz plot distribution bin by bin with the corresponding inverse value of the M.C. distribution. The resulting distribution, fig.9, shows a clear linear slope, $g = 0.54 \pm 0.17$, also of correct order of magnitude. So, in spite of the fact of quite large efficiency corrections and very rough and preliminary data handling, regarding corrections of measured energies, f.i., the slope factor seems to be rather insensitive.

Future plans

The next hardware improvement will be a buffer memory, now under construction, which was designed in order to improve the DAQ speed by at least a factor of 10. The description will be given elsewhere.

The next run is foreseen in the april 93 period, with the goal to record at least $15 \cdot 10^6$ triggers (with 2nd level trigger and negative beam). This would, with the present overall efficiency of 0.5% , correspond to nearly twice the world statistics on the $K^- \rightarrow \pi^-\pi^0\pi^0$ decay.

While this measurement is certainly worth doing (see the discussion in the introduction), the possibility of attacking the problem of direct CP-violation has to be reconsidered in the light of present theoretical and experimental knowledge. This requires an updated proposal, which will be prepared by the TNF collaboration in order to make a new decision.

Figure captions

Fig.1: Slope asymmetry Δg in charged K–decays, related to $\frac{\epsilon'}{\epsilon}$ as a function of m_{top}

Fig.2: Distribution of (longitudinal) z-coordinates of vertices
a) for minimum bias triggers
b) for M.C. generated $K^{\pm} \rightarrow \pi^{\pm}\pi^{0}\pi^{0}$ decays

Fig.3: π^0–mass distribution from $K^{\pm} \rightarrow \pi^{\pm}\pi^{0}$ decays
a) unselected
b) with cut $p_T < 0.05 GeV/c$ on residual momentum
c) after background subtraction

Fig.4: Difference of generated and reconstructed projected angles for
a) x–plane
b) y–plane

Fig.5: π^0–mass resolution $\frac{\Delta m}{m}$ as a function of π^0–energy (GeV) for the energy resolution constant
$C = 0.1\sqrt{GeV}$ (———)
$C = 0.2\sqrt{GeV}$ (- - - - -)

Fig.6: Hardware trigger signal from the e.m. calorimeter vs. analogous value from software (vertical scale)

Fig.7:
a) Efficiency distribution for Y from M.C.
b) Y–distribution from run 34 (2nd–level trigger)
Both distributions are weighted with inverse Dalitz–plot contour.

Fig.8: Graph of S(g)

Fig.9: Y–distribution taken from 7.b), efficiency corrected with 7.a)

References

[1] TNF-coll., preprint PHE 90-07,(1990).

[2] TNF-coll., Proposal "Search for direct CP-violation...at the IHEP 70 GeV accelerator", DESY Internal Report, 1992.

[3] A.A.Bel'kov, G.Bohm, D.Ebert and A.V.Lanyov, Phys. Lett. B232 (1989) 118.

[4] H.-Y.Cheng, Phys. Rev. D44 (1991) 919.
G.D'Ambrosio, G.Isidori and N.Paver, Phys. Lett. B273 (1991) 497.
G.Isidori, L.Maiani and A.Pugliese, Preprint INFN n.848, Roma 1991.

[5] A.A.Bel'kov, G.Bohm, D.Ebert, A.V.Lanyov and A.Schaale, Phys. Lett. B300 (1993) 283.

[6] G.Buchalla, A.J.Buras and M.K.Harlander, Nucl. Phys. B337 (1990) 313.

[7] A.A.Bel'kov, D.Ebert, A.V.Lanyov and A.Schaale, Preprint PHE 91-08, Zeuthen, 1991.
Int. Jour. Mod. Phys. A, 1993.

[8] B.Grinstein, S.J.Rey and M.B.Wise, Phys.Rev.D33 (1986) 1495

[9] J.Kambor, J.Missimer and D.Wyler, Phys.Lett.B261 (1991) 496.

[10] T.J.Devlin and J.O.Dickey, Rev. Mod. Phys. 51 (1979) 237.

[11] Particle Data Group, Phys. Lett. B239 (1990) 1.

[12] L.Wolfenstein, Phys.Rev.Lett. 13 (1965) 562.

Fig. 1

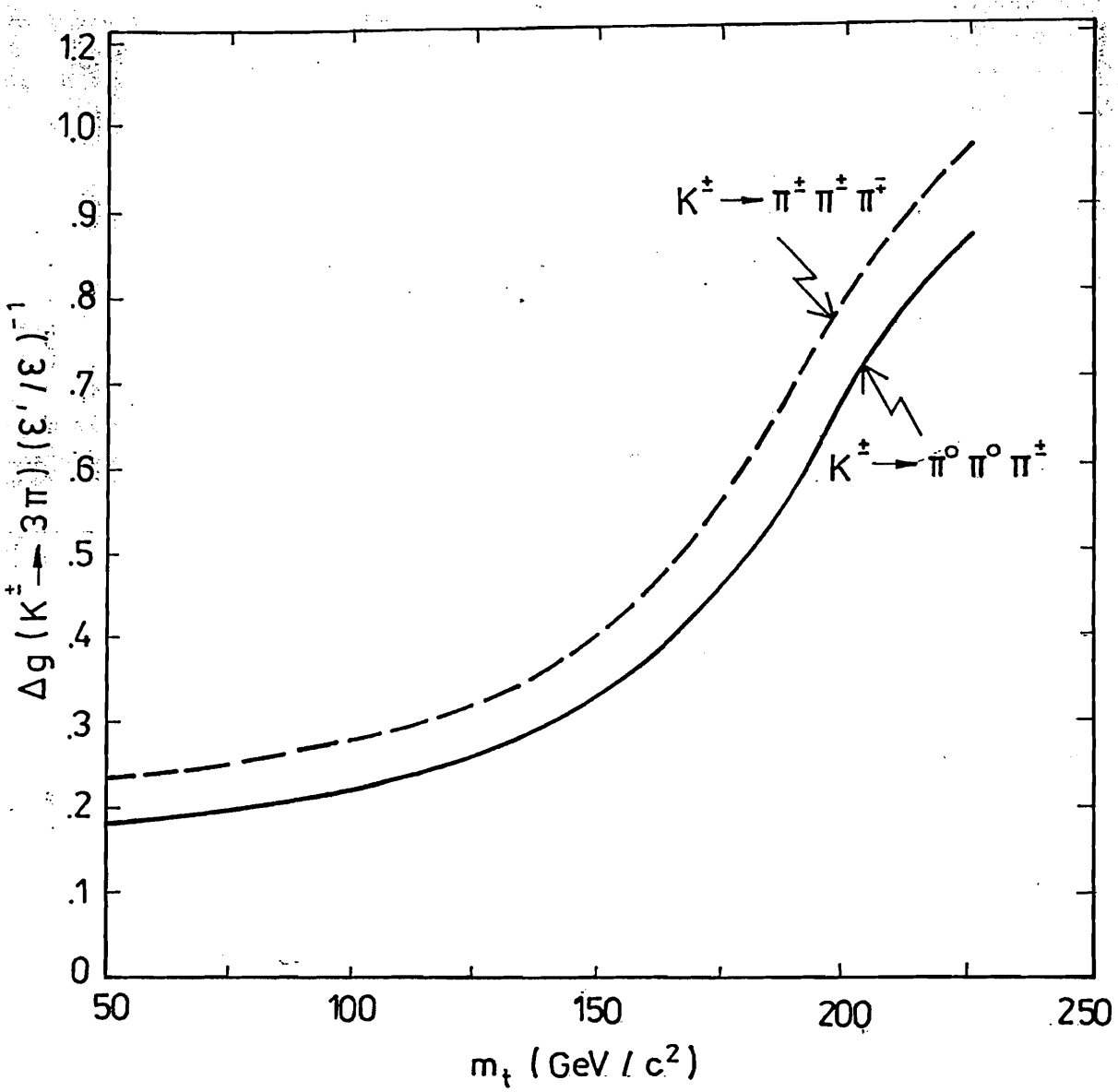
1.2
1.0
.9
.8
.7
.6
.5
.4
.3
.2
.1
0
50
100
150
200
250
$\Delta g\,(K^{\pm} \to 3\pi)\,(\varepsilon'/\varepsilon)^{-1}$
m_t (GeV / c^2)
$K^{\pm} \to \pi^{\pm}\pi^{\pm}\pi^{\mp}$
$K^{\pm} \to \pi^{0}\pi^{0}\pi^{\pm}$

Fig 2a

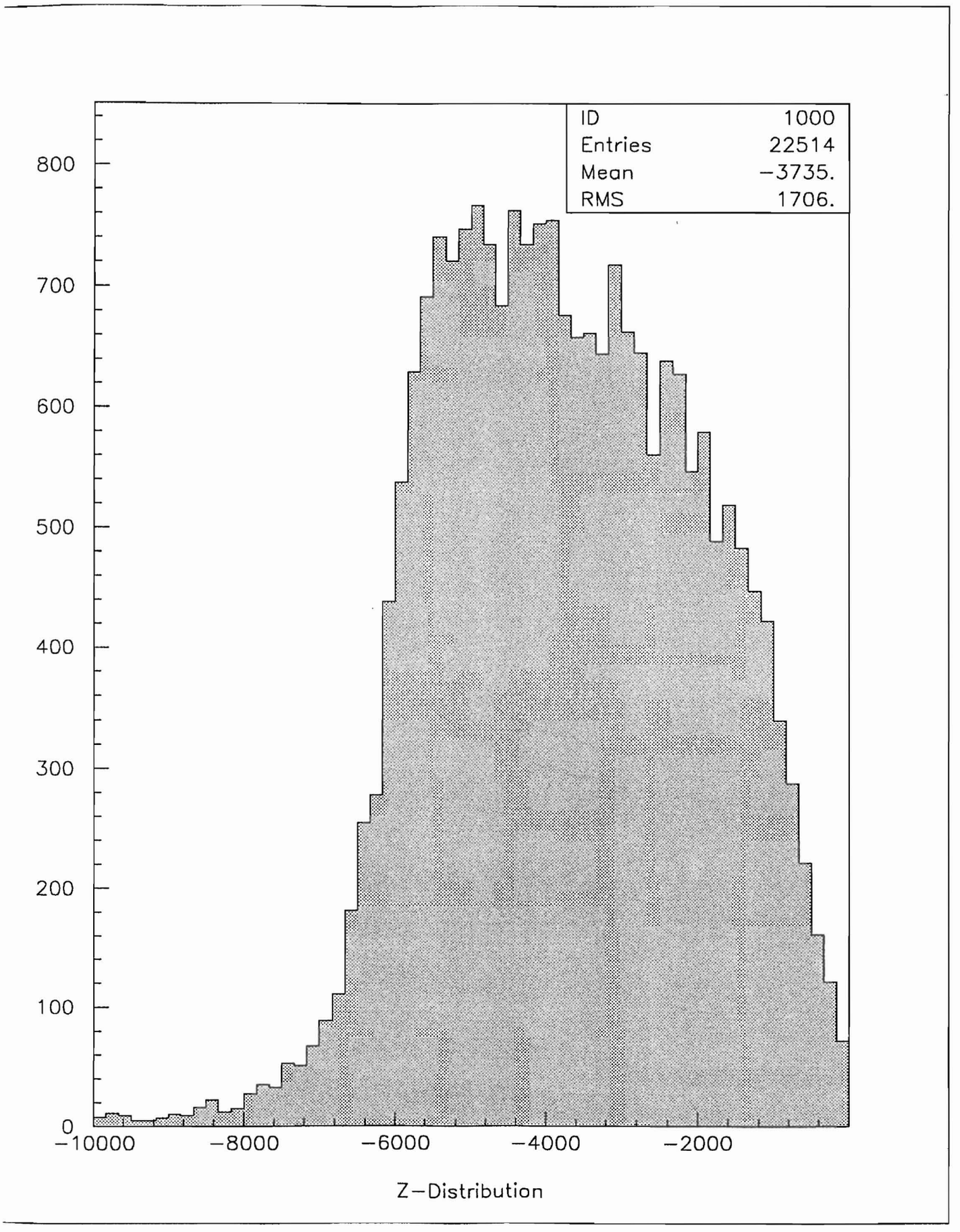
ID 1000
Entries 22514
Mean −3735.
RMS 1706.
800
700
600
500
400
300
200
100
0
−10000
−8000
−6000
−4000
−2000
Z−Distribution

Fig. 2b

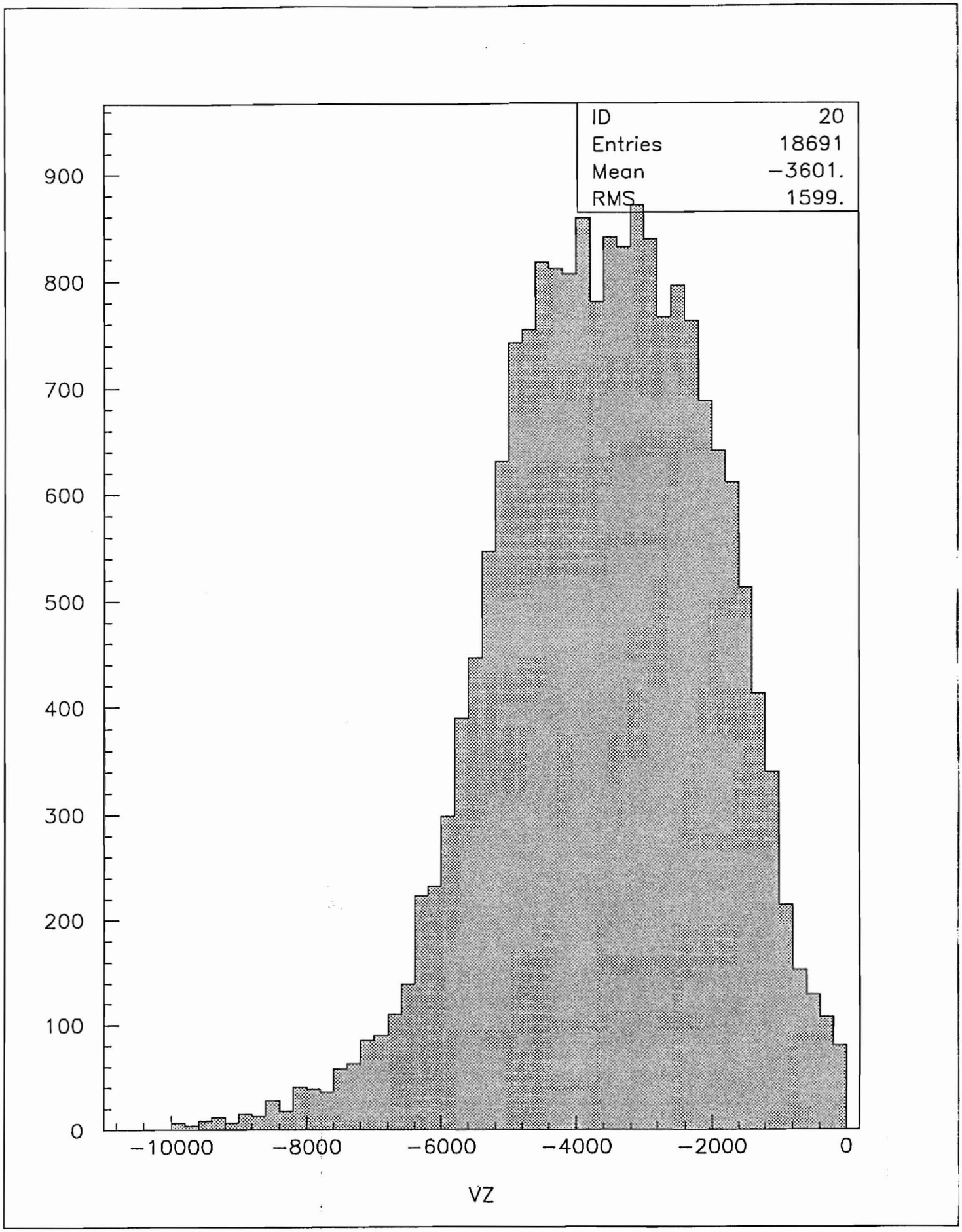
ID 20
Entries 18691
Mean −3601.
RMS 1599.
900
800
700
600
500
400
300
200
100
0
−10000
−8000
−6000
−4000
−2000
0
VZ

Fig. 3a

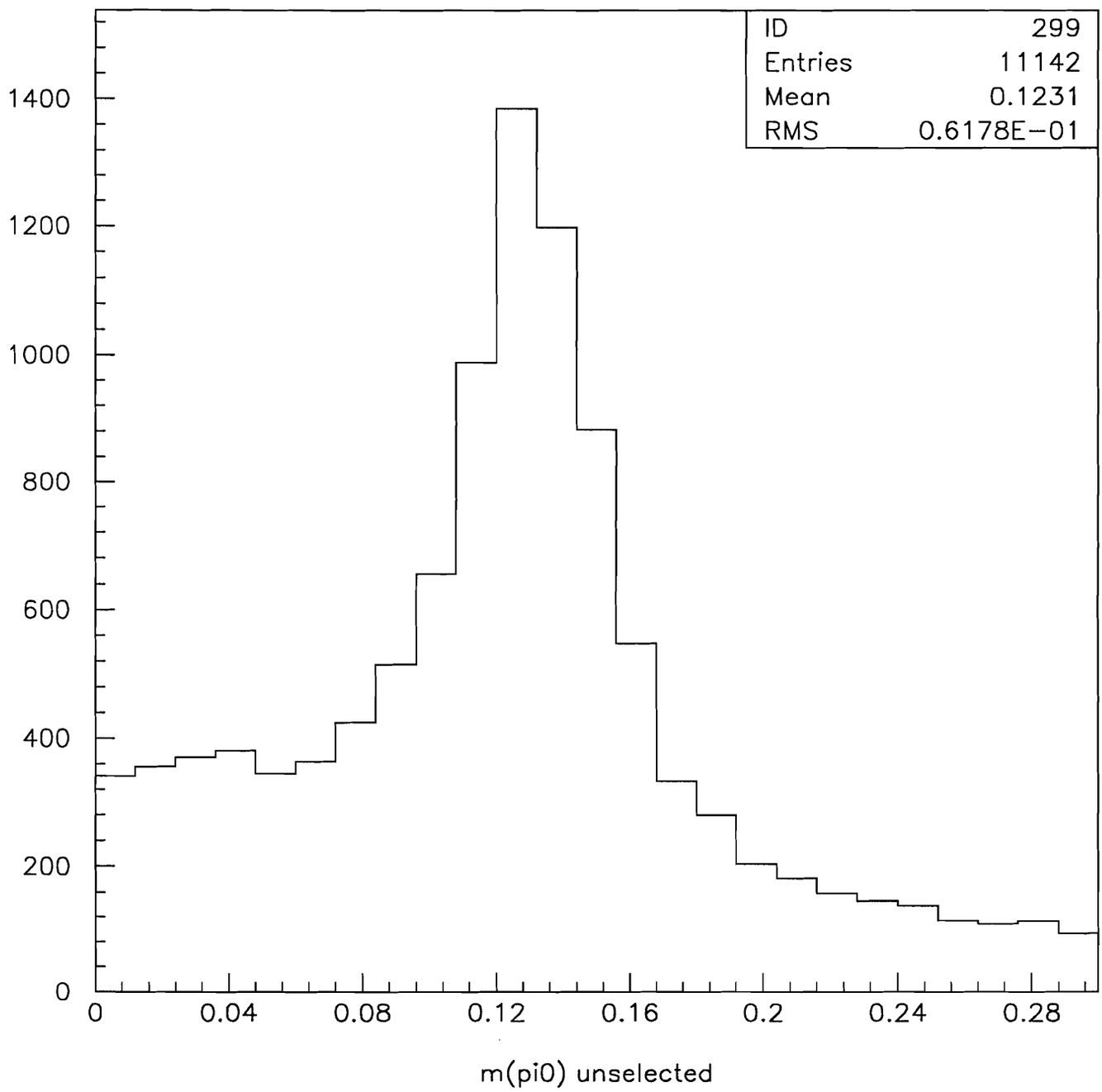
ID 299
Entries 11142
Mean 0.1231
RMS 0.6178E−01
1400
1200
1000
800
600
400
200
0
0
0.04
0.08
0.12
0.16
0.2
0.24
0.28
m(pi0) unselected

Fig. 3b

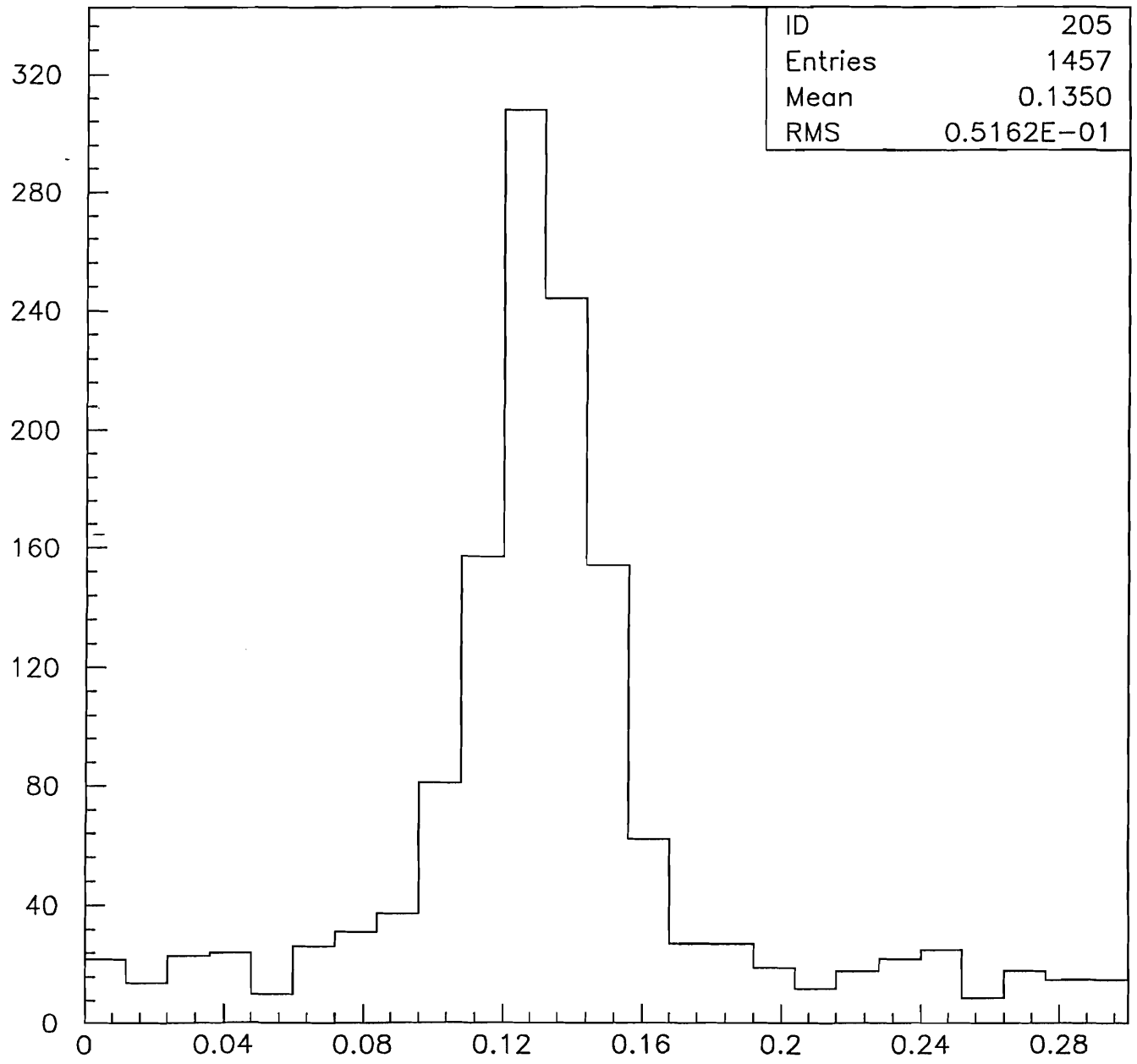

m(pi0) selected AND with momentum corr cut=0.05 $|\Delta p_T| < 50$ MeV

Fig. 3c

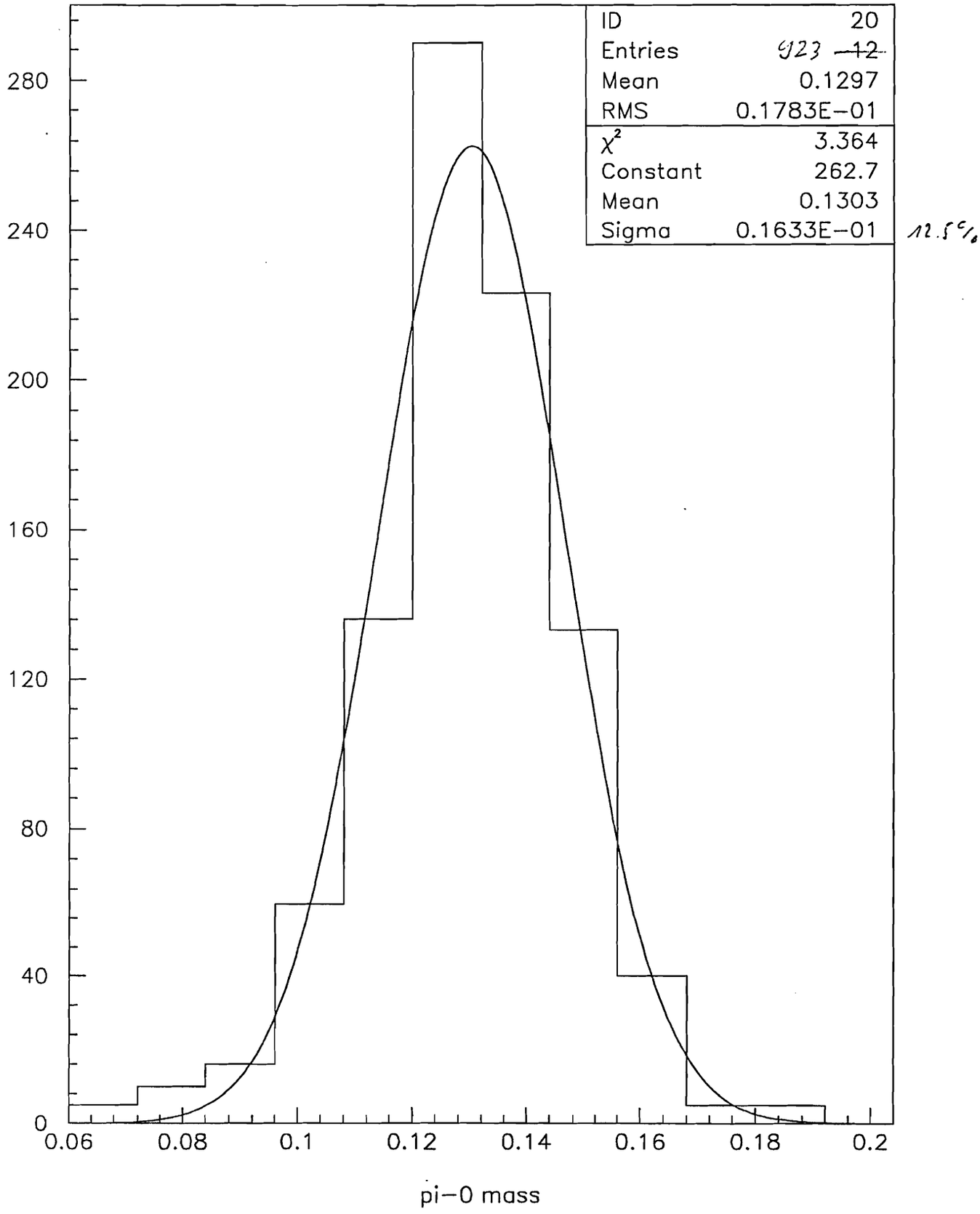
ID 20
Entries 923 ~~12~~
Mean 0.1297
RMS 0.1783E−01
χ^2 3.364
Constant 262.7
Mean 0.1303
Sigma 0.1633E−01
12.5%
280
240
200
160
120
80
40
0
0.06
0.08
0.1
0.12
0.14
0.16
0.18
0.2
pi−0 mass

Fig. 4a

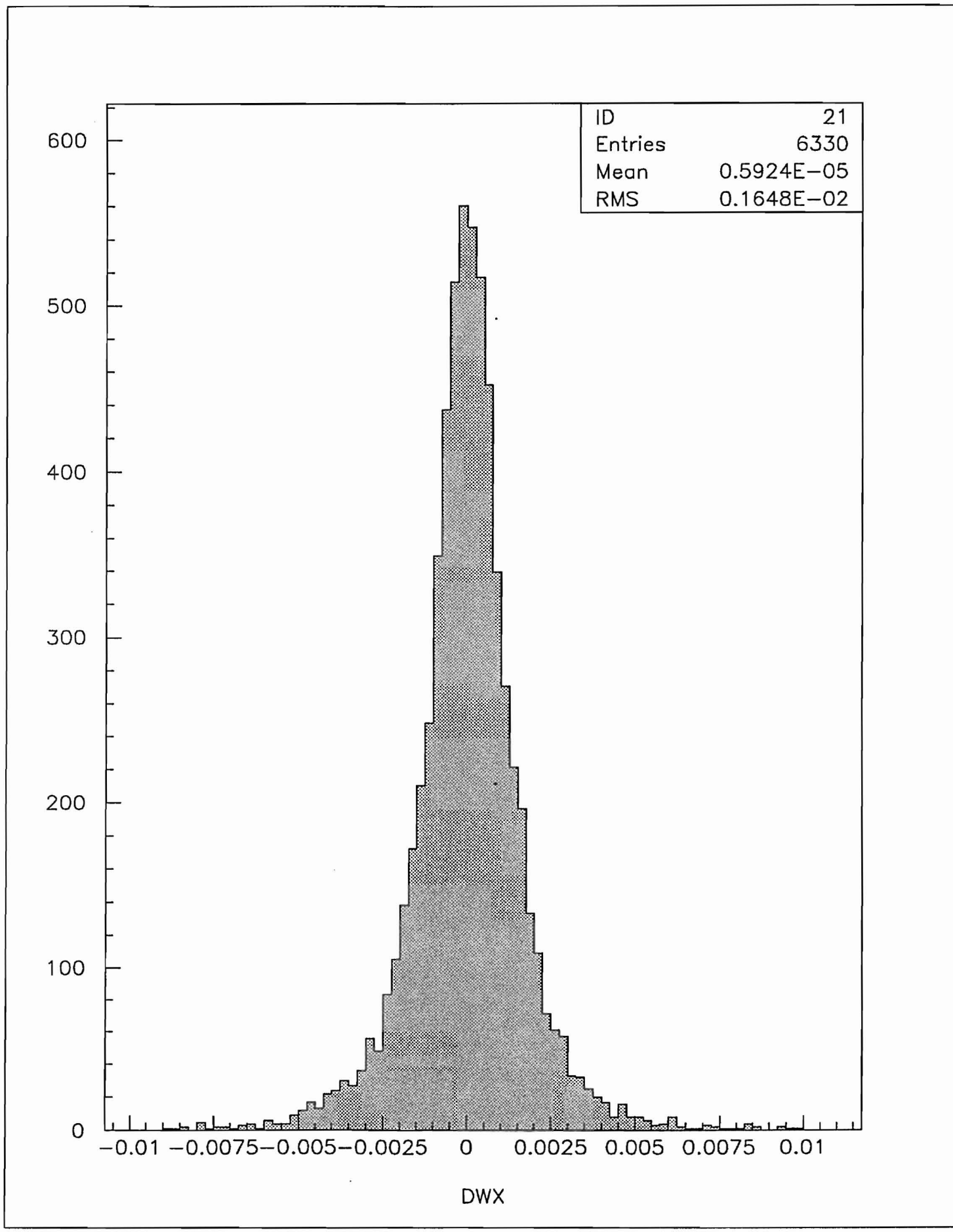
ID 21
Entries 6330
Mean 0.5924E−05
RMS 0.1648E−02
600
500
400
300
200
100
0
−0.01 −0.0075 −0.005 −0.0025 0 0.0025 0.005 0.0075 0.01
DWX

Fig. 4b

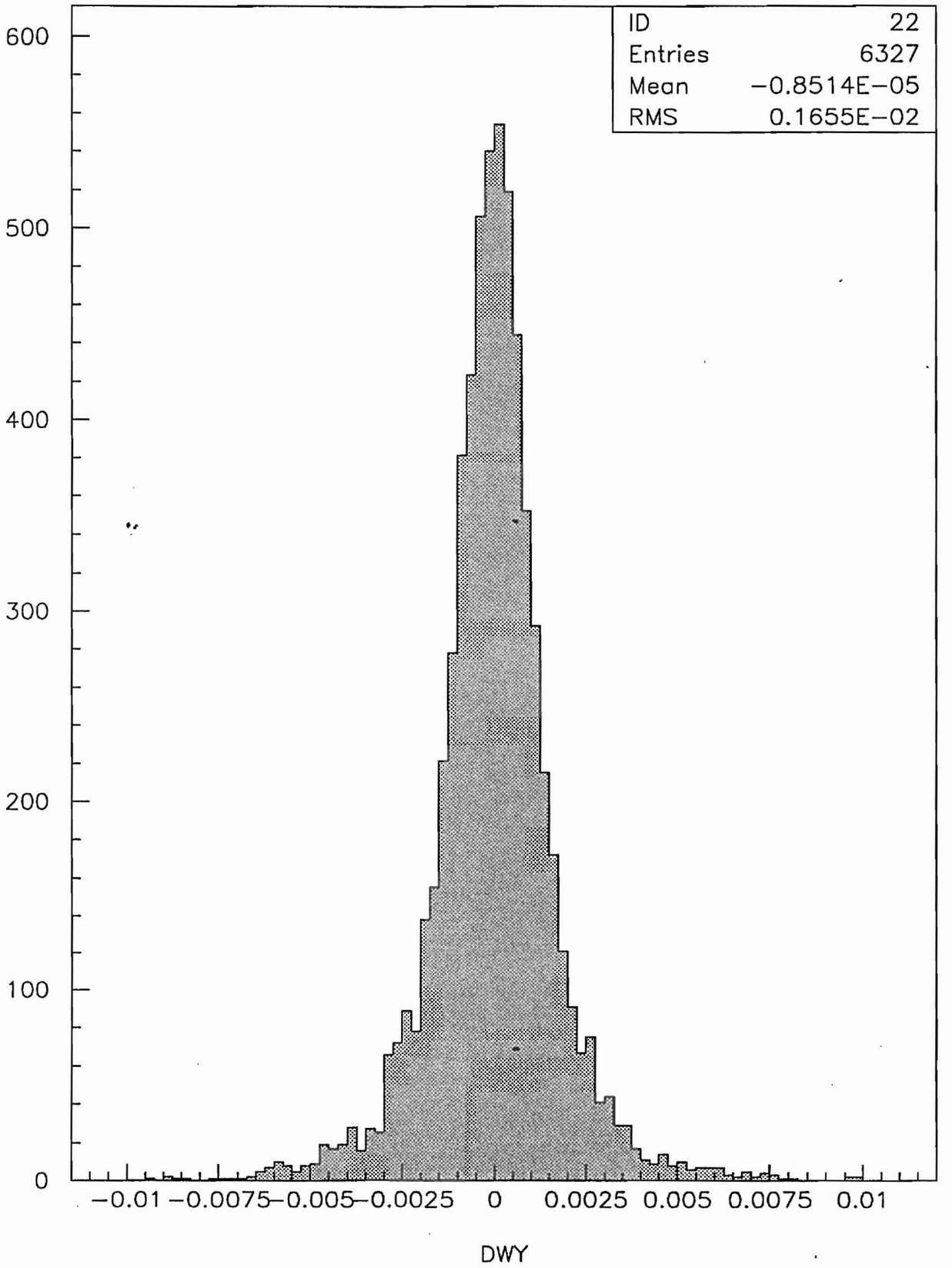
ID 22
Entries 6327
Mean −0.8514E−05
RMS 0.1655E−02
600
500
400
300
200
100
0
−0.01 −0.0075 −0.005 −0.0025 0 0.0025 0.005 0.0075 0.01
DWY

Fig. 5

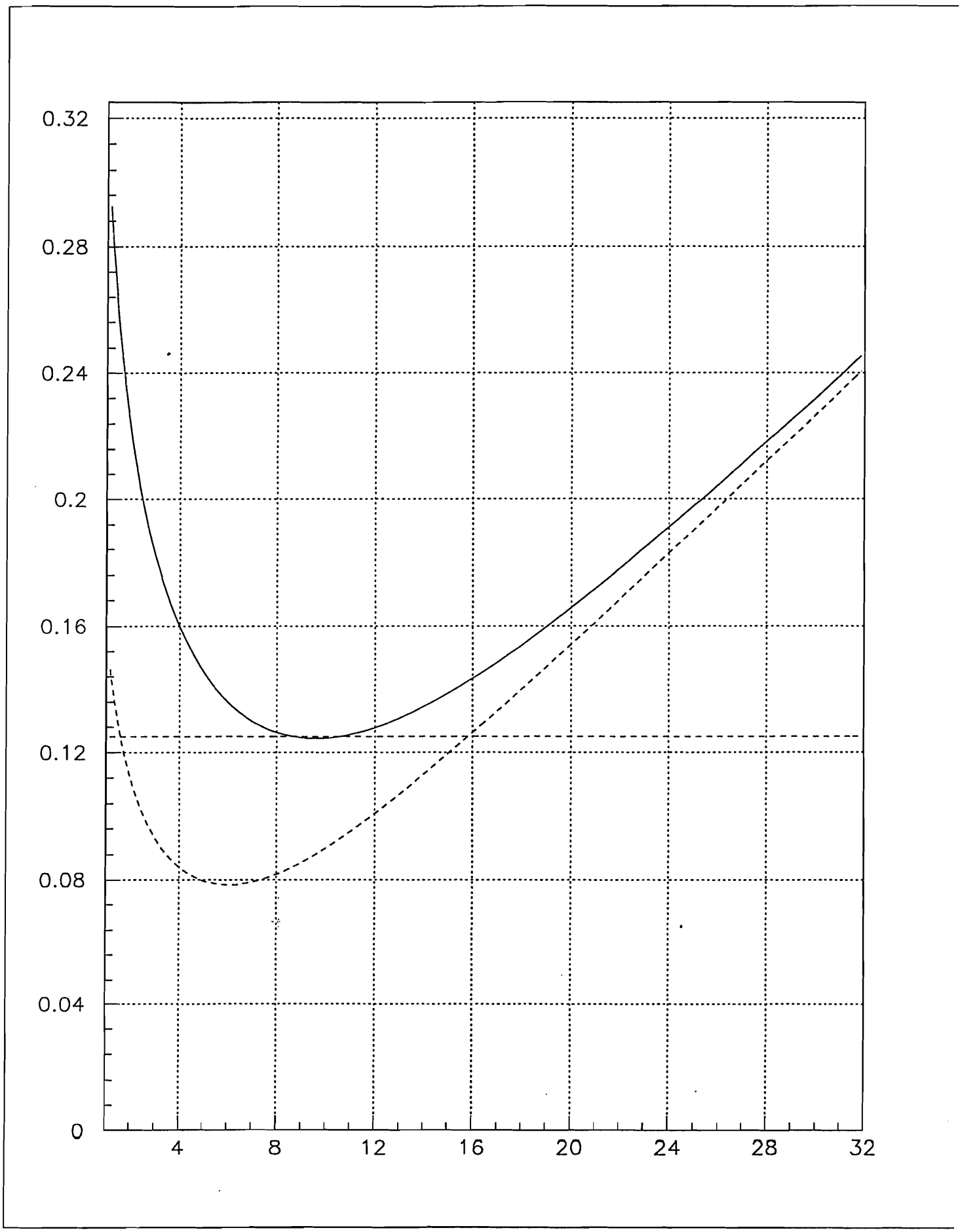

Fig. 6

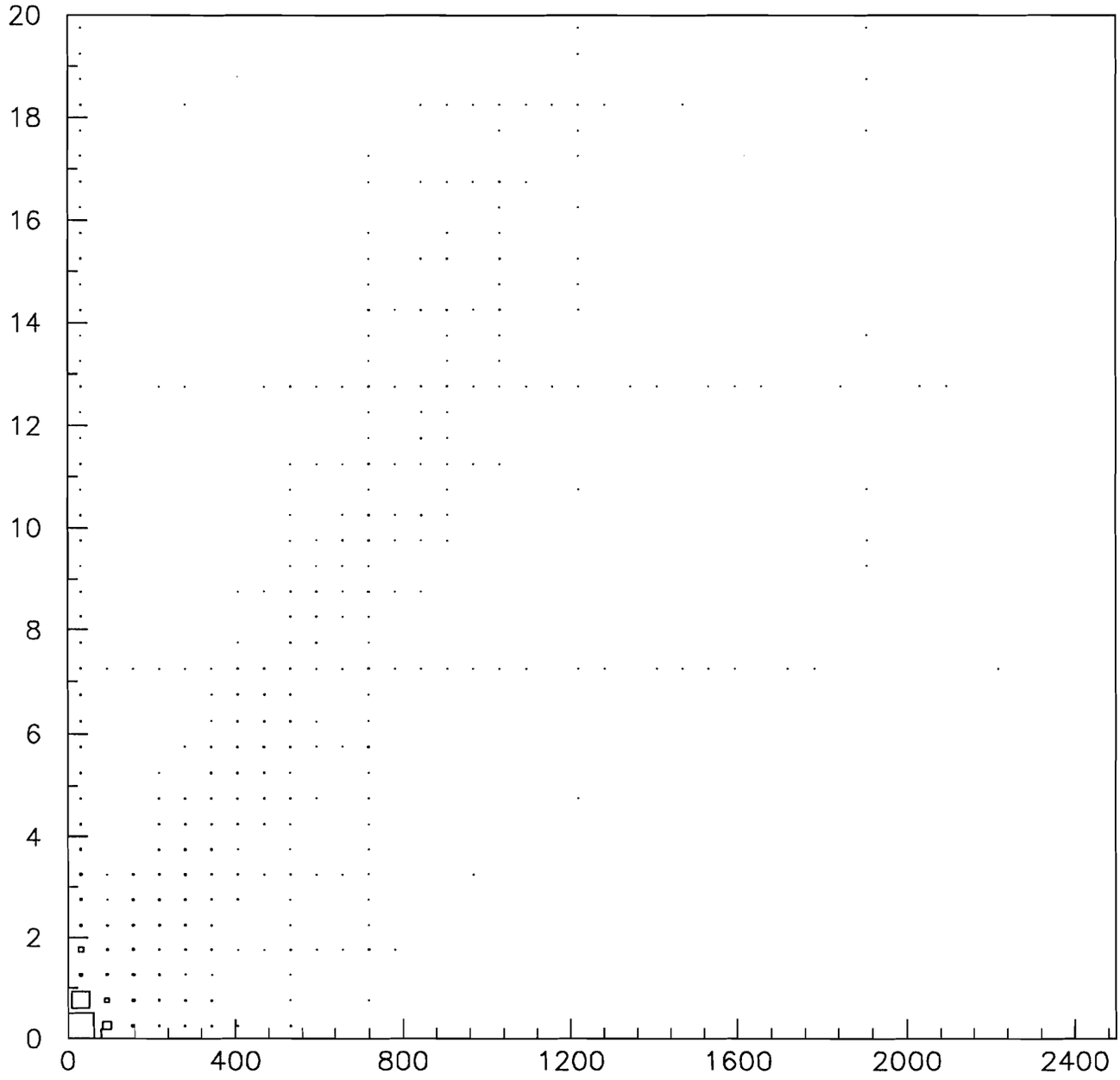

ISIG vs EHEX

Fig. 7a

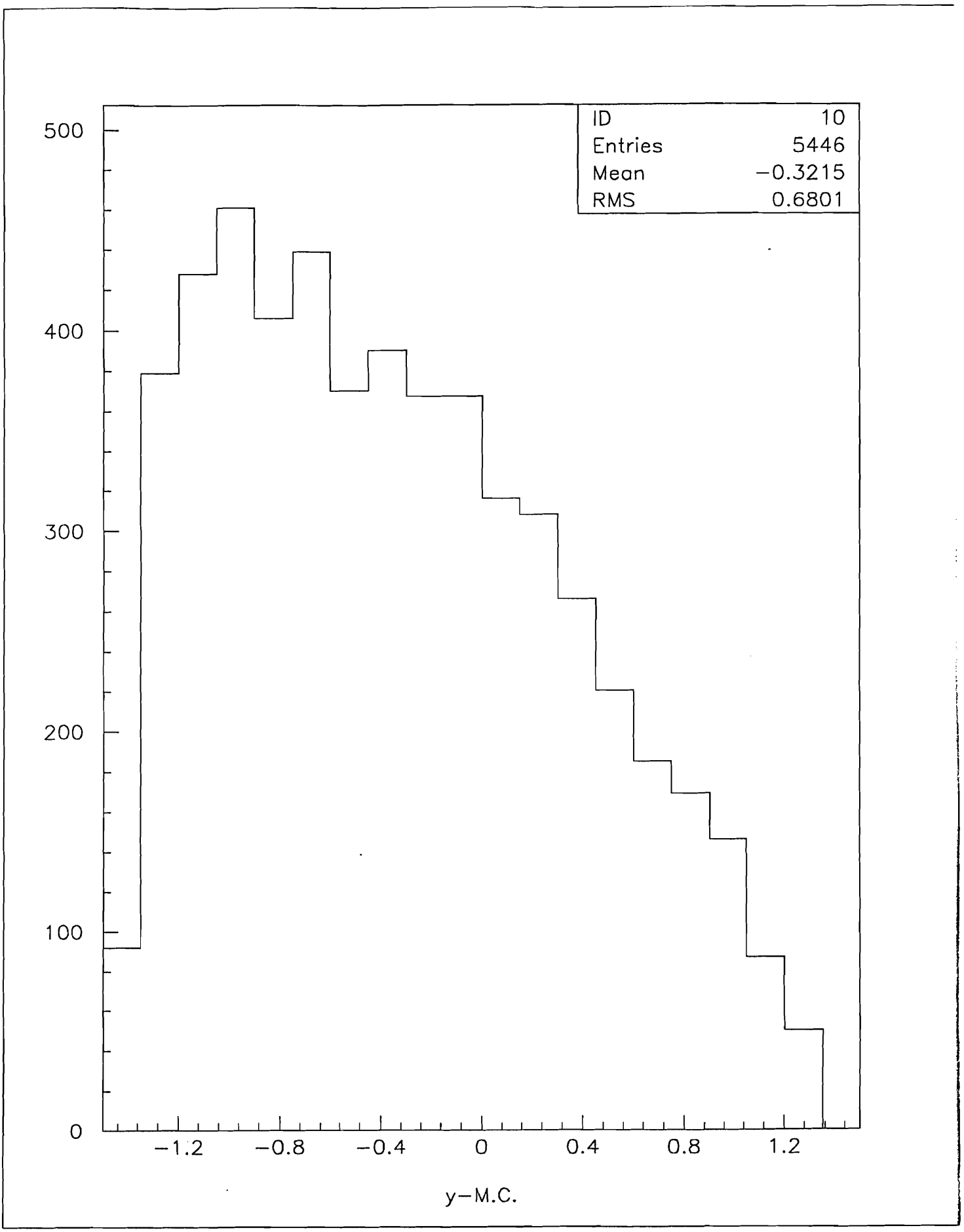
ID 10
Entries 5446
Mean −0.3215
RMS 0.6801
500
400
300
200
100
0
−1.2
−0.8
−0.4
0
0.4
0.8
1.2
y−M.C.

Fig. 7b

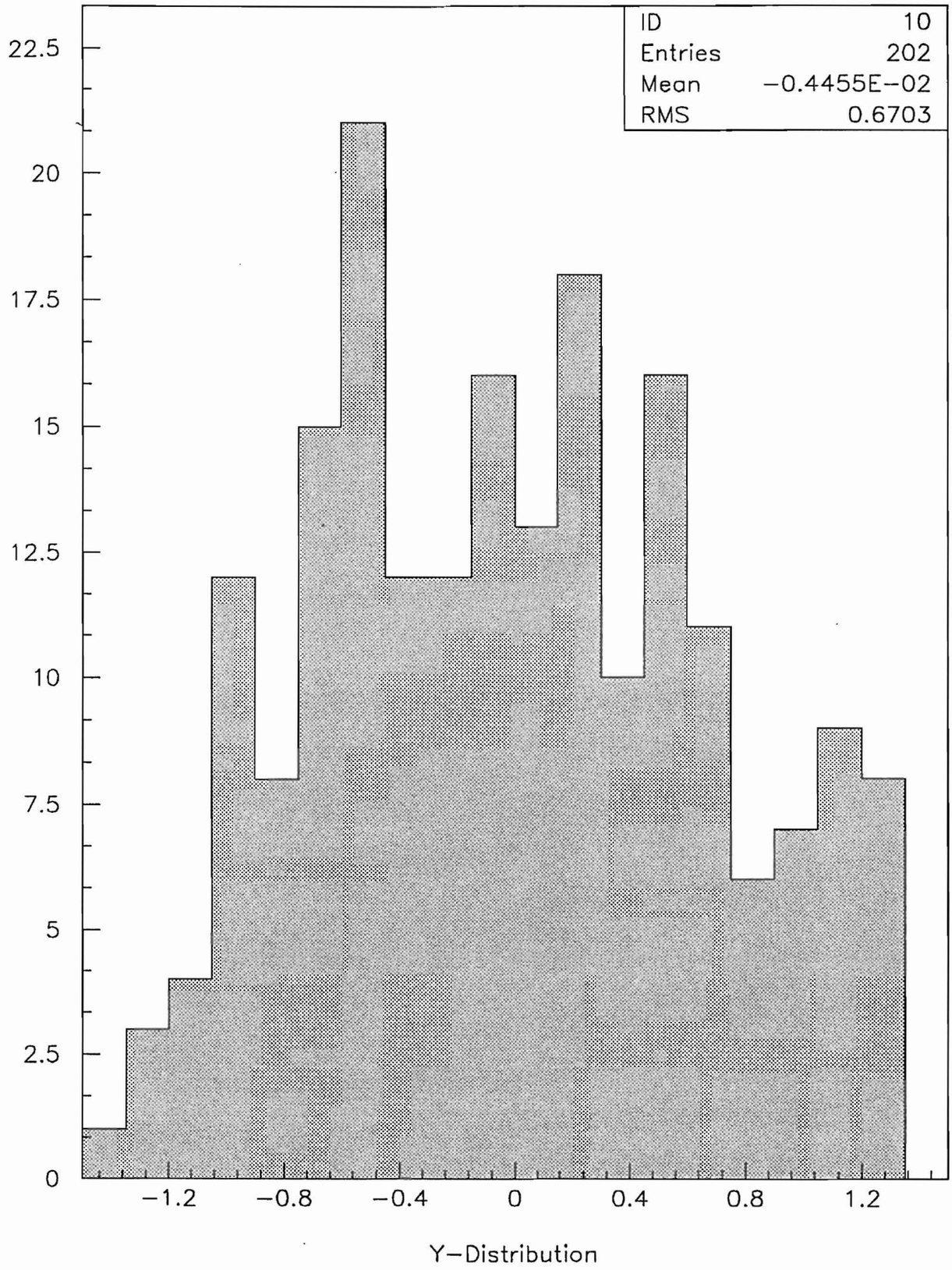
ID 10
Entries 202
Mean −0.4455E−02
RMS 0.6703
22.5
20
17.5
15
12.5
10
7.5
5
2.5
0
−1.2
−0.8
−0.4
0
0.4
0.8
1.2
Y−Distribution

Fig. 8

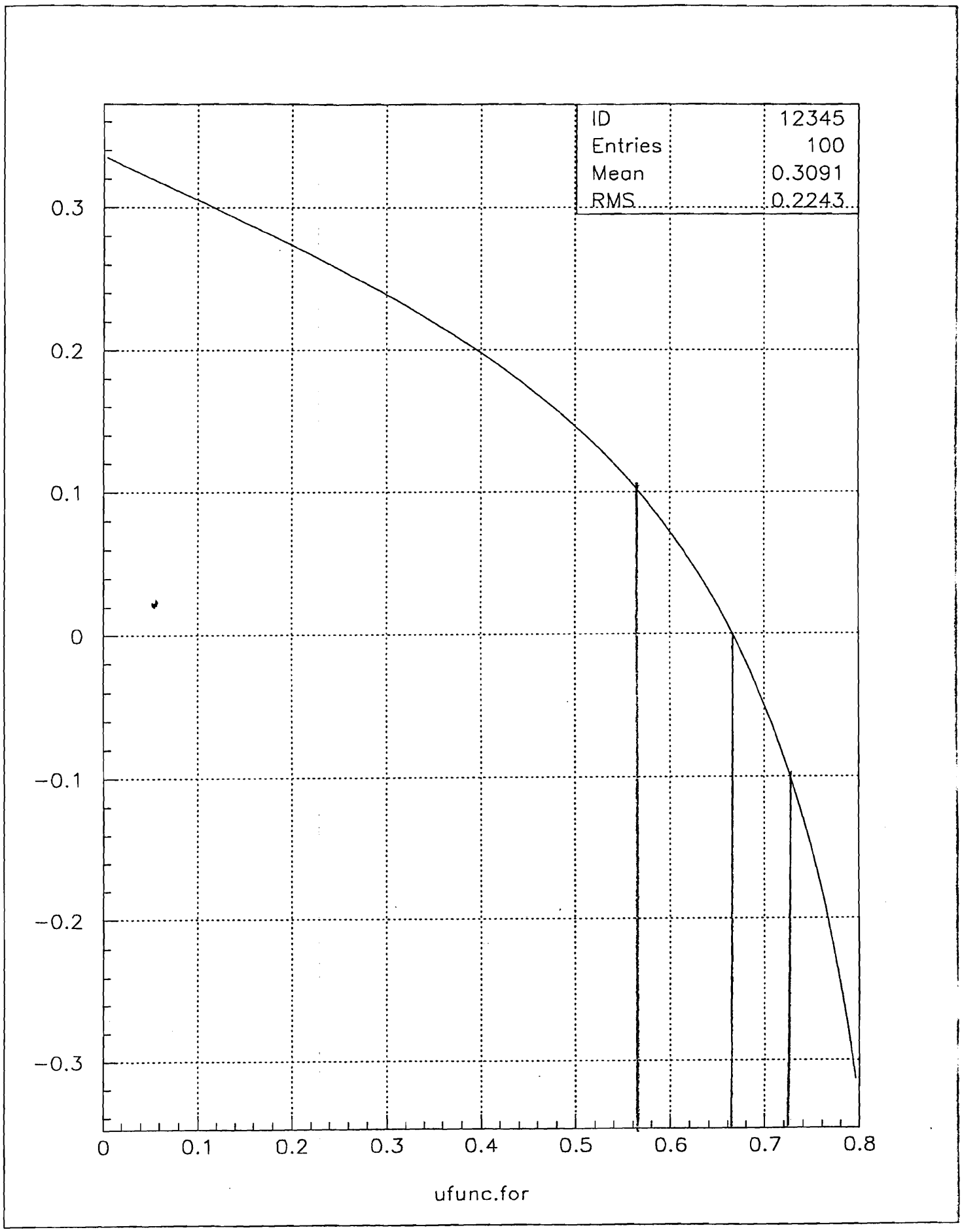
ID 12345
Entries 100
Mean 0.3091
RMS 0.2243
0.3
0.2
0.1
0
−0.1
−0.2
−0.3
0
0.1
0.2
0.3
0.4
0.5
0.6
0.7
0.8
ufunc.for

Fig 9

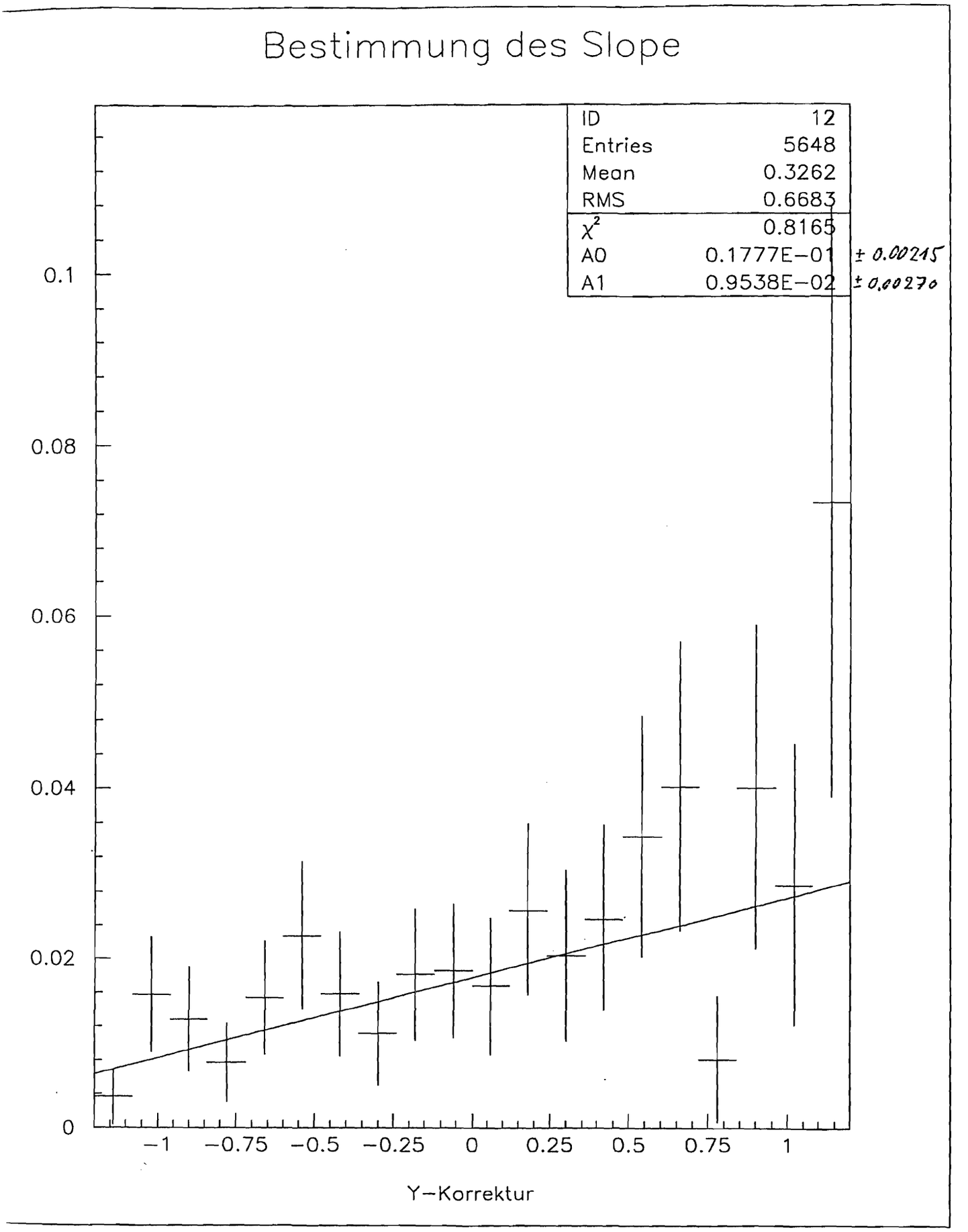
Bestimmung des Slope
ID 12
Entries 5648
Mean 0.3262
RMS 0.6683
χ² 0.8165
A0 0.1777E−01 ± 0.00215
A1 0.9538E−02 ± 0.00270
0.1
0.08
0.06
0.04
0.02
0
−1
−0.75
−0.5
−0.25
0
0.25
0.5
0.75
1
Y−Korrektur